Low UV-C stress modulates Chlamydomonas reinhardtii biomass composition and oxidative stress response through proteomic and metabolomic changes involving novel signalers and effectors

Francisco Colina
Universidad de Oviedo
María Carbó
Universidad de Oviedo
Mónica Meijón
Universidad de Oviedo
María Jesús Cañal
Universidad de Oviedo
Luis Valledor (valledorluis@uniovi.es)
Universidad de Oviedo https://orcid.org/0000-0002-0636-365X

Research

Keywords: Chlamydomonas, UV-C, biomass, ROS, sugars, metabolomics, proteomics, systems biology

Posted Date: March 11th, 2020

DOI: https://doi.org/10.21203/rs.3.rs-16852/v1

Version of Record: A version of this preprint was published on June 19th, 2020. See the published version at https://doi.org/10.1186/s13068-020-01750-8.

Abstract

Background The exposition of microalgae and plants to low UV-C radiation dosages can improve their biomass composition and stress tolerance. Despite UV-C shares these effects with UV-A/B but at much lower dosages, UV-C sensing and signal mechanisms are still mostly unknown. Thus, we have described and integrated the proteometabolomic and physiological changes occurring in Chlamydomonas reinhardtii – a simple Plantae model– into the first 24 h after a short and low intensity UV-C irradiation in order to reconstruct the microalgae response system to this stress.

Results The microalgae response was characterized by increased redox homeostasis, ROS scavenging and protein damage repair/avoidance elements. These processes were upregulated along others related to the modulation of photosynthetic electron flux, antenna size, carbon fixation and C/N metabolism. These changes, attributed to either direct UV-C-, ROS- or redox unbalances-associated damage, trigger a response process involving novel signaling intermediaries and effectors as the translation modulator FAP204, a PP2A like protein and a novel DYRK kinase. These elements were found linked to the modulation of Chlamydomonas biomass composition (starch accumulation) and proliferation, within an UV-C response probably modulated by different epigenetic factors.

Conclusion Chosen multiomics integration approach was able to describe many fast changes, including biomass composition and ROS stress tolerance, as a response to a low intensity UV-C stress. Moreover, the employed omics and systems biology approach placed many previously unidentified protein and metabolites at the center of these changes. These elements would be promising targets for the characterization of this stress response in microalgae and plants and the engineering of more productive microalgae strains.

Background

Plants and microalgae are well adapted to surface and underwater UV-A/B irradiation, with specific sensing systems allowing the deployment of different acclimation and photomorphogenic responses. Many of these responses involve changes in their biomass composition and their resistance to stress [1,2]. UV-C, with a minor incidence in the natural environment, produces similar biomass, stress and development effects over plants [3,4] and microalgae [5–7] but at a much lower dosage. Despite this, UV-C sensing and signal mechanisms remain obscure and is unclear if they are specific or rather shared with other stressors. Therefore, the characterization of the signal elements involved in the UV-C modulation of biomass composition and stress resistance is needed and would contribute to the generation better microalgae strains and plant varieties.

UV-C perception and signaling converge with UV-A/B in the generation of damaging Reactive Oxygen Species (ROS), key stress signals [8] related in turn to other signalers as Ca^{2+}, salicylic acid (SA), jasmonates (JA) and abscisic acid (ABA) [3,4] which are known to contribute in the responses to UV and other stressors. On the other hand, in land plants as Arabidopsis thaliana –hereafter Arabidopsis– and

microalgae species as Chlamydomonas reinhardtii –hereafter Chlamydomonas– the perception an signaling of UV-A and UV-B radiations also relies on specific photoreceptors as the UV-B specific UVR8 [1,2]. This receptor however is insensitive to UV-C [9] and no specific one has been identified for this radiation. The different signaling pathways associated to UV stress response operate through the regulation of epigenetic mechanisms which in turn play an important role in the control of the final UV responses. Under UV-B, UVR8 induces HISTONE H3 Lys 9/Lys 14 (H3K9/K14) acetylation over its regulated gene loci [10]. Moreover UV-C has been associated to changes in the global DNA methylation levels [11].

UV-C induces many changes in the expression of different plant and microalgae genes related to stress response. One of these changes output is the enhancement of plant and microalgae tolerance to stress. The increased tolerance is behind the accumulation of valuable and protective compounds including lipids –mostly polyunsaturated fatty acids, carotenoids and sterols– and UV-shielding compounds –flavonoids and mycosporine-like amino acids–, and the enhancement of stress responsive mechanisms as ROS scavenging enzymes [5–7,12]. Many of these effects are similar to those induced by UV-A and/or UV-B treatments [2,13,14]. All these UV effects have promising biotechnological applications, especially for microalgae, where UV-C benefits do not stop at the modulation of these organism's biomass profile but also can contribute to their rapid settling. Thus, the usage of this radiation would avoid costly manipulations related to biomass harvesting and/or the substitution of culture medium while increasing these organisms biomolecule yield [5]. UV-C has enhancing effects on biomass composition in industry relevant species as Haematococcus pluvialis and Dunaliella salina –enhancing lipids and carotenoids synthesis– [6], and different crop species –by the starch accumulation– [15–17], remaining the molecular mechanisms behind this response unknown. The closeness of these Chlamydomonadal species to the chlorophyte model Chlamydomonas, with its multiple available genomic/proteomic resources and simpler plant-like UV-A/B signaling pathways, makes this microalga the selected model for the characterization of this response. Then, key response proteins derived from these results, could be translated into more productive microalgae strains.

The aim of this study is to render an image of the changes in the Chlamydomonas stress response system during the first 24 h after a short and low intensity UV-C irradiation. These changes would be identified through the description of the change of different microalgae physiological parameters and the integration of its proteome and metabolome changes under the initial stage of the stress response. This integration, compared to similar transcriptome and physiology-based approaches over Chlamydomonas UV-B response [1], involves novel omic data processing strategies combining the prediction of interaction between the described omic levels with existing interaction knowledge. This approach has allowed the identification of key factors related to UV-C signaling mechanisms and metabolic responses including those related with the modulation of the microalgae biomass composition.

Results

Physiological characterization of Chlamydomonas response to UV-C stress

A small number of physiological parameters were measured along experiment (Additional file 1: Table S3). The radiation had a negative effect over the microalgae photosynthetic parameters, with the reduction of Fv/Fm ratio, but also increased Chlorophyll b concentration at t 24 h, reducing the Chla/b ratio (ANOVA 0.05) (Fig. 1a). Low UV-C doses enhance the accumulation of photoprotective photosynthetic pigments in other industry relevant microalgae close to Chlamydomonas [5,6]. Cultures cellular density and biomass (FW) increased after the exposition to a low UV-C dose, however, cellular density had a transient drop 5 h after irradiation. UV-C stress also modified the microalgae biomass composition with the accumulation of starch and the fall of soluble sugars upon stress imposition (ANOVA 0.05) (Fig. 1b). This starch accumulation is also observed in UV-C irradiated crop species as sugar beet [15], potato [16], and lily bulb [17].

Integrated proteomic and metabolomic responses on Chlamydomonas exposed to UV-C stress

Proteomic analysis allowed the identification of 1441 protein species in whole cell protein extracts. After data pre-processing, 885 proteins were above the abundance threshold for confident quantitation (Additional file 1: Table S1). GC-MS allowed the unequivocal identification of 69 primary metabolites, out of these 68 were considered for quantitative purposes (Additional file 1: Table S2). Detected proteins and metabolites were classified according to MapMan V4 categories [18], and 703 proteins and 54 metabolites were assigned to functional bins. These bins comprised 27 pathways for proteins and 8 for metabolites, covering different cellular processes. Out of these, 398 proteins and 14 metabolites could be considered quantitatively differential in at least one sampling time ANOVA, 0.05 (5% FDR for protein variables) (Additional file 1: Table S1, S2).

Heatmap clustering based on MapMan-categories distinguished the different treatments with an adequate grouping of samples (Fig. 2). At protein level (Fig. 2a) UV-C stress induced a quick reduction on multi process regulation, RNA processing, Protein biosynthesis and Cell cycle related categories, all classified in the same meta group. On the other hand, the abundance of Protein degradation, External stimuli response, Carbohydrate metabolism and Cellular respiration categories, within the same cluster, increased after 5 h. Interestingly, Redox homeostasis increased 24 h after stress start when Photosynthesis bin reached its maximum abundance. Metabolites (Fig. 2b) showed a divergent distribution to those of proteins, highlighting Amino acid and Carbohydrate metabolism categories time shifts with their protein counterparts. Within individual metabolites, amino acids and organic acids as serine, glutamine, and malic and citric acids down-accumulated upon stress imposition (Fig. 3a), while redox-related glycerol, arabinose and 4-hydroxybenzoic acid accumulated after 5 h (Fig. 3b). On the other hand, the increase of several unknown sugars abundance after 24 h characterized acclimation (Fig. 3c) (Additional file 1: Table S1, S2).

Samples were correctly classified by PCA when considering each omic level independently (Additional file 2: Figure S1; Additional file 1: Table S4, S5). In proteomics dataset (Table 1, Additional file 2: Figure S1a; Additional file 1: Table S4) principal component 1 (PC1) potentially gathers variability related to the photoacclimation to UV-C, while principal component 2 (PC2) collects early response elements. At

metabolome level (Additional file 2: Figure S1b; Additional file 1: Table S5) PC1 explain early response with the enhancement of secondary metabolism; while PC2 joins late accumulated sugars.

Table 1. List of all the high-ranking Chlamydomonas proteins in the PCA analysis with a key role in the microalgae response to UV-C stress.

	Loadings					
Accession	PC1	PC2	qvalue	Abundance	Symbol	Defline
Cre03.g199983.t1.1	-0.049	-0.010	0.000		PP2A	Ser/Thr protein phosphatase
Cre12.g558100.t1.2	-0.050	-0.012	0.000		PRMT2	Protein-/Histone-arginine N-methyltransferase
Cre07.g356600.t1.2	-0.051	-0.011	0.000		MINA53	MINA53 MYC INDUCED NUCLEAR ANTIGEN
Cre11.g467689.t1.1	-0.037	0.008	0.031		PETC	Chloroplast cytochrome b6f Rieske subunit
Cre09.g393200.t1.2	-0.006	0.066	0.000		HSP70C	Heat shock protein 70C
Cre17.g721500.t1.2	0.005	0.060	0.000		STA2	Granule-bound starch synthase I
Cre01.g022500.t1.2	0.017	0.065	0.031		MME5	NADP malic enzyme
Cre09.g394850.t1.2	0.010	0.061	0.048		TEF24	LrgB-like protein
Cre01.g045550.t1.2	0.014	0.052	0.041		APE2	solute carrier family 35 protein
Cre13.g567600.t1.2	0.016	0.048	0.000		COX4	Mitochondrial cytochrome c oxidase subunit
Cre16.g671000.t1.2	0.018	0.065	0.000		NDA5	Type-II NADH dehydrogenase
Cre06.g261500.t1.2	0.010	0.047	0.000		CPLD58	Conserved in the Plant Lineage and Diatoms
Cre06.g274650.t1.1	0.020	0.058	0.000		NUOAF4	Complex I associated CIA30 protein
Cre01.g025250.t1.1	0.017	0.057	0.000		RFK2	Riboflavin kinase
P09144	0.023	0.062	0.003		psaB	PSI P700 chlorophyll a apoprotein A2
P06007	0.036	0.031	0.039		psbD	Photosystem II D2 protein
Cre03.g189800.t1.2	0.043	0.009	0.031		CYN38	Peptidyl-prolyl cis-trans isomerase
Cre17.g720250.t1.2	0.046	-0.016	0.024		LHCB4	Light-harvesting protein of PSII
Cre08.g370450.t1.2	0.042	-0.029	0.000		MGE1	Mitochondrial GrpE homolog
Cre12.g560950.t1.2	0.046	-0.036	0.006		PSAG	Photosystem I reaction center subunit V
Cre06.g256250.t1.2	0.043	-0.021	0.043		TEF14	Thylakoid lumenal protein
Cre03.g182551.t1.2	0.043	-0.024	0.024		PCY1	plastocyanin, chloroplast precursor
Cre11.g476750.t1.2	0.030	-0.060	0.048		FNR1	Ferredoxin-NADP reductase, chloroplast
Q32065	0.032	-0.059	0.045		FTSH	Uncharacterized 341.7 kDa protein
Cre02.g084500.t1.1	0.026	-0.056	0.000		CGL134	possible phytol kinase
au5.g1142_t1	0.029	-0.060	0.000		DYRK	Ser/thr protein kinase, DYRK like

Protein accession is followed by their loadings in the first (PC1) and second (PC2) components of the PCA analysis, their abundance change between the three measured time points, and the protein symbols and defline.

A protein-metabolite correlation network was also defined (Fig. 4b) through the integration of both datasets employing sPLS regression (Fig. 4a, Additional file 1: Table S6). This correlation network was overlapped to the STRING network of the correlation network nodes. Within the resulting network sPLS-STRING (Fig. 4b) the cluster centered on early depleting metabolites (citrate, malate, glutamate, dehydroascorbate) and early accumulated arabinose gathered multiple proteins depleting upon stress start and related to translation (ribosomal subunits); cellular respiration and carbon metabolism-related PYRUVATE KINASE (PYK2), ISOCITRATE LYASE (ICL2) and multiple mitochondrial respiratory chain subunits; and development/stress-related MYC INDUCED NUCLEAR ANTIGEN (MINA53) and PHOSPHATASE 2A (PP2A) homolog Cre03.g199983.t1.1. STRING respectively highlighted the interaction between the depleting mitochondrial and ribosomal subunits and the links of the later to the different and also early depleting translation initiation factors. Moreover, these translation-related proteins were predicted to be associated to the PP2A homolog.

STRING linked the early depleting PP2A and ribosome subunits cluster and also translation-related FLAGELLAR ASSOCIATED PROTEIN 204 (FAP204) to different early accumulated aminoacyl tRNA synthetases (TSM2, TSL1, SYK1) and the EUCARIOTIC TRANSLATION INITIATION FACTOR 1A (EIF1a). TSM2, TSL1, SYK1 and EIF1a were included along other early (t 5 h) accumulated elements into a cluster centered on early accumulated glycerol including redox and carbon fixation RIBOFLAVIN KINASE (RFK2), GLUTATHIONE S-TRANSFERASE homolog (CPLD58), AQUAPORIN (MIP1), NDA5, and MME5; translation modulation S-ADENOSYL-L-METHIONINE-DEPENDENT METHYTRANSFERASE (SAM MTase) and signaling (WD40 REPEAT PROTEIN) elements. STRING highlighted the possible interactions between the WD40 REPEAT PROTEIN and the early depleted development/stress-related MINA53. Glycerol cluster correlated negatively to another cluster with elements accumulated after 24 h centered in UNKNOWN SUGAR 5. Fatty acid (FA) synthesis B-KETOACYL-[ACYL-CARRIER-PROTEIN] SYNTHASE III (KASIII) (Cre04.g216950.t1.2) and a DYRK like kinase (Cre01.g008550.t1.1 or au5.g1142_t1) positively correlated to the late accumulated sugar. A novel FILAMENTOUS TEMPERATURE SENSITIVE H like (FTSH) like protease connected the cluster centered on early depleted elements with the clusters gathering elements accumulated after 5 and 24 h of UV-C irradiation.

Since protein-metabolite interactions in the sPLS-STRING network (Figure 4b) were only based on mathematical models, STITCH analysis was applied to improve these interactions based on biological models (Additional file 2: Figure S2). STITCH network highlighted early accumulated glycerol connections to protein biosynthesis, respiration and lipid metabolism along the mentioned STRING protein-protein interactions.

UV-C irradiation affects mitochondrial electron transport enhancing ROS production and inhibiting oxidative phosphorylation

Mitochondrial respiration and ATP synthesis downregulated under UV-C stress with the depletion of multiple subunits of respiratory and F_1F_0 ATP synthase complexes, excepting the early accumulated IV subunit (COX4) (Table 1, Additional file 1: Table S1). Interestingly, UV-C treatment increased the abundance of chaperones associated to respiratory complexes. NUOAF4, chaperone of the large complex I, was exclusively detected on early stress response and HSP70C, a subunit of the IV associated HSP70 complex, peaked at this stage (1-fold at t 5 h) (Table 1, Additional file 1: Table S1). HSP70 complex can aggregate with MGE1 and COX4, also up-accumulated under stress (Table 1, Additional file 1: Table S1), allowing the incorporation of COX4 into the IV complex [19]. Moreover, the accumulation of HSP70C has been described in response to heat stress induced protein misfolding in Chlamydomonas [20]. UV irradiation effect over mitochondrial proteins also triggers ROS bursts [8]. ROS scavenging catechin, catechin biosynthesis related CHALCONE ISOMERASE (Cre12.g517100.t1.1) and redox related TCA ISOCITRATE DEHYDROGENASE (IDH2) accumulated under UV-C (0.8-, 1.5-, 2.2-fold at t 24 h) (Table 1, Additional file 1: Table S1, S2). Moreover, also redox related RIBOFLAVIN KINASE (RFK2) was exclusively detected under early stress (Table 1, Additional file 1: Table S1). RFK overexpression protect human cells from oxidative stress enhancing GSH metabolism [21].

Low intensity UV-C irradiation modulates thylakoid electron transport and fixed carbon allocation under inhibited respiration

Tested radiation damaged chloroplastic proteins, especially those of antenna and PSII as showed by the reduction of Fv/Fm ratios (Figure 1B, Supplementary table S3). Enhanced damage was linked to an increase in protein turnover and protection. Central photosystem II (PSII) PsbD subunit (D2) peaked under early response along PSI P700 CHLOROPHYLL A APOPROTEIN A2 (psaB) (0.9-, 2.4-fold at t 5 h) and antennal CHLOROPHYLL a-b BINDING PROTEIN CP29 (LHCB4) up-accumulated under stress (1-fold at t 24 h) (Table 1, Additional file 1: Table S1). Chlamydomonas LHCB4 is a key modulator of non-photochemical quenching (NPQ) and state transitions [22]. The accumulation of D2 and LHCB4 proteins matched the accumulation of a FTSH-like chloroplastic protease (Q32065) (Table 1, Additional file 1: Table S1), working together as a photosynthetic protein protection and turnover mechanism [23–25]. These photosynthetic protein turnover and protection-related elements accumulated along others associated to the repair and assembly of photosynthetic complexes as the THYLAKOID LUMINAL FACTOR (TEF14), CYN38 and CHLOROPLASTIC DNAJ-LIKE PROTEIN (CDJ1) (2.7-, 2.4-, 1.2-fold respectively at t 24 h) (Table 1, Additional file 1: Table S1). Arabidopsis mutants on TEF14 and CYN38 orthologs fail to assembly and repair PSII [24,26]. Chlamydomonas CDJ1 organizes chloroplast HSPs under heat stress [27] and its accumulation under UV-C points to an enhanced protection of photosynthetic proteins and complexes. The accumulation of CDJ1 under stress matched the early accumulation of the mitochondrial HSP70C chaperone but no chloroplastic HSPs accumulated. Thus, these changes suggest that the tested low UV-C dosage damages PSII, triggering different measures to avoid and repair damage matching the late accumulation of chlorophyll b and the associated decrease of antenna size-related Chl a/b ratio (Figure 1a, Additional file 1: Table S3).

Response to chloroplastic UV-C damage also involved the accumulation of the PSI stabilizing PSI reaction center subunit V (psaG), FERREDOXIN NADP REDUCTASE (FNR1) and PLASTOCYANIN (PCY1) (2.7-, 1-, 1.6-fold at t 24 h) (Table 1, Additional file 1: Table S1). The accumulation of these proteins – involved in both Linear and Cyclic Electron Flow (LEF and CEF)– and the enhanced PSI/II turnover and protection are compatible with an enhancement on LEF and or CEF on acclimation. In spite of this, CEF/LEF-related CYTOCHROME b6f RIESKE IRON-SULFUR CENTER SUBUNIT (PETC) down-accumulated on acclimation (-9.6-fold at t 24 h) and Fv/Fm ratio did not recover control values (Table 1, Figure 1a, Additional file 1: Table S1, S3). On the other hand, LEF and CEF happens as independent processes in Chlamydomonas, where supercomplexes of PSI, Cytb6f and FNR are exclusively dedicated to the later [28]. PSI subunits and FERREDOXIN NADP REDUCTASE (FNR1) accumulated under stress and other subunits associated to this complex as PETO, PGRL1, Cyt b6 and Cyt f maintained their abundance (Additional file 1: Table S1). This CEF-associated complex assemblies under reducing conditions, performing Fd-CEF where FNR consume NADPH to reduce Ferredoxin and contribute to the production of ATP [29].

The fall of Fv/Fm and Chl a/b ratios, the accumulation of NPQ/state transition-related antennal protein LHCB4, and the diverging changes in the abundance of LEF/CEF-related proteins matched early changes

in the chloroplastic redox homeostasis. Redox modulates Chlamydomonas CEF rate, carbon metabolism and ROS scavenging mechanisms. NDA5 oxidoreductase, whose Arabidopsis homolog (NDC1) is a chloroplastic/mitochondrial NADPH-dependent quinone oxidoreductase [30,31], and tocopherol biosynthesis PHYTOL KINASE (CGL134) were exclusively detected at t 5 and t 24 h respectively (Table 1, Supplementary Table S1). Detected catalases and peroxidases, related to the detoxification of H_2O_2 and superoxide radicals did not change their abundance on stressed samples (Additional file 1: Table S1). UV stress increases the production of superoxide radicals over singlet oxygen, which is the predominant reactive oxygen species under high light stress [32]. In spite of this, a novel protein containing a GLUTATHIONE-S-TRANSFERASE domain (CPLD58) was detected exclusively after 5 h of stress. A glutathione peroxidase and a glutathione-s-transferase drive the Chlamydomonas detoxification response to the increased production of singlet oxygen under high light stress [33]. Applied UV-C dosage rapidly and transiently enhanced the tolerance of the treated cells to rose Bengal (RB)-induced singlet oxygen ($^1O_2$) oxidative stress. Cells from the t 5 h harvest were able to survive on 2 □M RB while cells from the t 24 h harvest showed an oxidative stress tolerance close to those of unstressed cells, unable to grow on those RB concentration (Fig. 5). *D. salina* and *H. pluvialis* accumulate singlet oxygen scavenging carotenoids and malondialdehyde (MDA) –a lipid peroxidation product– under UV-C stress [6]. Strawberry plants exposed to UV-C, experiment a transient increase in their antioxidant capacity [34]. Other redox regulators as THIOREDOXIN M (TRXm) accumulated under stress (2.5-fold at t 24 h). On the other hand, redox regulated chloroplastic protein NADP MALATE DEHYDROGENASE (MME5) accumulated exclusively under early stress (5-fold at t 5 h) (Table 1, Additional file: Table S1). This enzyme is part of the malate shuttle, transferring not only carbon but excess reducing power from chloroplast to cytoplasm and other organelles.

The early accumulation of redox/carbon-related MME5 concurred with the accumulation of glycerol (0.7-fold at t 5 h) (Fig. 3, Additional file 1: Table S2). Glycerol synthesis is an ATP producing and NADH consuming fermentative process. Moreover, glycolate/glycerate (TEF24), triose phosphate:Pi (APE2) antiporters accumulated under stress (2.9-, 4-fold respectively at t 5 h) and glycerol transporter (MIP1) was exclusively detected at t 5 h (Table 1, Additional file 1: Table S1). On the other side, OPP 6-PHOSPHOGLUCONATE DEHYDROGENASE (GND1), a NADPH producing enzyme also accumulated on t 5 h (1.3-fold). Arabidopsis GND1 homolog (PGD) accumulate under ROS stress providing the required NADPH for the ROS scavenging mechanisms [35]. RuBisCO large subunit (RBCL) also accumulated on t 5 h (1-fold at t 5 h) (Additional file 1: Table S1). Low intensity UV treatments increase microalgae RuBisCO content and activity [36]. Besides this, RuBisCO small subunit isoform 1 (RBCS1) depleted under stress. Interestingly, RuBisCO small subunit isoform 2 (RBCS2) abundance did not change under stress (Supplementary Table S1). Starch accumulated under stress (Fig. 1b) along many enzymes related to their synthesis as GRANULE BOUND STARCH SYNTHASE (STA2) (2.1-fold at t 5 h) and STARCH BRANCHING ENZYME (SBE3), accumulated at t 5 h. Enhanced starch synthesis matched the down-accumulation of soluble sugars (Fig. 1b), the late accumulation of Glucose and unknown sugars as UNKNOWN SUGAR, UNKNOWN SUGAR 4 and UNKNOWN SUGAR 5 (1-, 1.2-, 1.2-, 1-fold at t 24 h) and the depletion of TREHALOSE-6-PHOSPHATE SYNTHASE (TPS) (Table 1, Figure 3b, Additional file 1: Table S1,

S2). TPS produces trehalose-6-phosphate (T6P), an inhibitor of the SnRK1 kinase, a key node in plant carbon metabolism also influenced by the cellular redox status [37,38]. Sugars and starch also accumulated in UV-C treated lily bulb [17] and sugar beet [15].

The modulation of carbon metabolism was related to the increased protein turnover, involving an increased amino acid demand. Serine and Glutamate down-accumulated at t 5 h (-2.65-, -3.83-fold respectively) (Figure 3a, Additional file 1: Table S2), while many enzymes related to amino-acid biosynthesis as SERINE ACETYLTRANSFERASE (SAT3), SERINE and ALANINE GLYOXILATE TRANSAMINASES (SGA1, AGT2), ISOPROPYLMALATE DEHYDROGENASE (LEU3) accumulated under early response (2.3-, 1.5-, 1.8-, 3.6-fold at t 5 h). Other amino acid-related enzymes as OXOPROLINASE (Cre07.g325748.t1.1) were exclusively detected on t 5 h or as CYSTATHIONINE BETA LYASE (METC) and METHYLCROTONYL CoA CARBOXYLASE alpha subunit exclusively on stressed samples (Table 1, Additional file 1: Table S1).

Alternative signalers modulate cell proliferation, development and metabolism under UV-C

The observed changes in protein turnover/protection carbon metabolism and ROS/redox-related elements were coupled to rapid changes on the abundance of many development and translation-related proteins. sPLS-STRING network (Fig. 4b) clustered many of these and linked the WD40 REPEAT PROTEIN (Cre12.g495650.t1.2), accumulated exclusively at t 5 h, to development related MINA53 (Cre07.g356600.t1.2), down-accumulating under stress (Table 1, Additional file 1: Table S1). The mutation of the human homolog of MINA53, MINA53/RIOX2, inhibit DNA replication/repair mechanisms and cell proliferation in human cell lines [39]. MINA53 was also linked in the sPLS-STRING network (Fig. 4b) through C/N metabolism to JmjC protein JMJC DOMAIN CONTAINING PROTEIN 7 (Cre03.g175750.t1.2), also down-accumulating under stress. Arabidopsis homolog to JMJC DOMAIN CONTAINING PROTEIN 7, JMJ32, is a HISTONE H3 lysine 27 (H3K27) demethylase, while its human homolog is JMJD7, a lysyl hydroxylase. HISTONE-ARGININE N-METHYLTRANSFERASE (PRMT2) also depleted upon stress imposition (Table 1, Additional file 1: Table S1). The fluctuations in the abundance of these histone related proteins under UV-C suggest the importance of the epigenetic- and/or amino acid residue hydroxylation-based modulation mechanisms in stress responses. sPLS- STRING and STICH networks also highlighted the link between C/N metabolism and protein synthesis to early accumulated translation modulation-related elements as EIF1a, FAP204 and aminoacyl tRNA synthases, and to a signaling PP2A like protein (Cre03.g199983.t1.1), which were exclusively detected in control samples (Fig. 4b, Table 1, Additional file 2: Figure S2, Additional file 1: Table S1). This novel PP2A like phosphatase is homolog to several Arabidopsis PP2A which are key nodes in plant immunity integrating pathogen perception at membrane level with pathogen response at multiple levels including SA, ABA and TOR signaling and C/N metabolism modulation [40,41]. PP2As link to TOR allow these proteins to regulate cell growth in response to the environment [42]. Thus, the connection of PP2A to protein synthesis and C/N metabolism in the sPLS- STRING and STITCH networks (Fig. 4b, Additional file 2: Figure S2) is suggestive of the PP2A like protein mediated tuning of TOR pathway in UV-C stressed Chlamydomonas. More directly related to the modulation of carbon metabolism under stress, sPLS-

STRING network (Fig. 4b) highlighted a correlation between DYRK kinase (Cre01.g008550.t1.1 or au5.g1142_t1) and the production of sugars and glycerol. This DYRK kinase, registered as CMGC_DYRK-PRP4 in the iTAK database [43], accumulated 24 h after UV-C irradiation start (Table 1, Additional file 1: Table S1). Other Chlamydomonas DYRK as TAR1 and STD1 are known for their roles in carbon storage under nutrient stress [44,45].

UV-C affected Chlamydomonas causing protein damage and ROS production. Results showed an early response to UV-C effects focused on damage avoidance through redox modulating, singlet oxygen focused ROS scavenging, and protein protection/turnover responses which concurred with the accumulation of starch. UV-C enhances ROS production in plants but also ROS scavenging mechanisms [4,8]. On the other hand, the acclimation stage was characterized by the modulation of carbon metabolism (accumulation of specific sugars and starch). Interestingly, UV-C treatments enhanced the synthesis of lipids in other microalgae species [5–7,12]. Late accumulated sugars and starch matched the up-accumulation of a DYRK kinase (Cre01.g008550.t1.1) whose homologs regulate carbon fluxes in Chlamydomonas [44,45]. Moreover, these responses are linked to protein expression/epigenetic modulation elements as MINA53 and PRMT2 that might be driving the proteogenomic changes after the observed UV-C adaptation and enhanced oxidative stress resistance in Chlamydomonas. All these elements would help for further UV-C stress characterization or exploitation towards the generation of enhanced strains.

Discussion

Chlamydomonas response to UV-C stress rely on redox modulation

Plants and also algae are exposed to ever changing light environments and continuously forced to adapt. For UV-C stress, adaption is focused on damage avoidance and repair mechanisms centered on photosynthesis and redox/energy metabolism modulation, and on the enhancement of protein turnover and ROS scavenging. Tested low UV-C radiation damaged Chlamydomonas photosystems as showed by the early downregulation of Fv/Fm ratio, and the evidence of an enhanced PSI/II protein turnover, protection and assembly. The accumulation of UV-sensitive PSI/II central and assembly-associated proteins and state transition-related antennal LHCB4, and the changes of antenna size-related Chl a/b ratio support the radiation effect on photosynthesis and the microalgae response focused on photoprotection and protein turnover. Although UV-C can directly damage macromolecules it is also an important source of ROS, whose scavenging is the other most relevant response. UV stress has been described as a generator of superoxide over other oxygen species as singlet oxygen, common in high light stress [32]. Interestingly, tested low UV-C dosage enhanced Chlamydomonas tolerance to exogenous RB induced singlet oxygen stress as well as the accumulation of possible singlet oxygen enzymatic scavengers as CPLD58, over H_2O_2 and superoxide scavenging enzymes. These changes suggested the importance of singlet oxygen stress at low UV-C dosages (Fig. 5, Additional file 1: Table S1). The generation of singlet oxygen is tightly related with the radiation effects over the chloroplast redox status and the photosensitizable chlorophylls [33]. On the other hand, the scavenging of these oxygen species

also relies on the chloroplast ability to generate ATP and reduced equivalents. The enhancement of chloroplastic ATP synthesis would be necessary as UV-C downregulated the mitochondrial electron transport and oxidative phosphorylation. The early enhance of chloroplastic ATP and NADPH producing pathways under UV-C, as glycerol synthesis and NADPH producing OPP enzyme GND1, and the possible late increase of CEF support the modulation of the chloroplastic energy/redox metabolism under this stress. These changes were tightly connected to the modulation of carbon fixation, metabolism and transport (Fig. 1-5, Additional file 1: Table S1, S2, S3). In Arabidopsis, the accumulation of ROS quenchers, as tocopherol was revealed as a key response against UV and light stresses derived ROS, contributing to the maintenance of PSII functionality [46]. The differential accumulation of enzymes related to the synthesis of tocopherol, the scavenging of ROS species (singlet oxygen) and to the modulation of reduced equivalents (NADPH) and thylakoidal reduced plastoquinone (PQH_2) pools, summarize the Chlamydomonas response to the increase of ROS and breakage of redox homeostasis under this stress.

UV-C induced non-enzymatic ROS scavenging mechanisms in Chlamydomonas through the accumulation of diverse phenolic compounds (4-hydroxybenzoic acid, catechin) and phenolic metabolism enzymes as CHALCONE ISOMERASE, the late accumulation of sugars, and the enhancement of tocopherols synthesis as suggested the accumulation of a predicted PHYTOL KINASE (CGL134) (Fig. 3, Additional file 1: Table S1, S2). Phenolic compounds and tocopherol are also accumulated in UV irradiated *Pinus radiata* plants [47]. The accumulation of soluble sugars is observed under different plant abiotic stresses associated to a ROS scavenging function [48,49]. Arabidopsis PHYTOL KINASE 1 (VTE5) participates in tocopherol synthesis through the recycling of phytol from degraded chlorophyll [50], thus the presence of a PHYTOL KINASE under UV-C also suggest UV/ROS damage to the antenna pigments. Photosynthetic antenna damage is commonly pointed out by an increase in the Chl a/b ratio after the reduction of chlorophyll b abundance, exclusively present into the antenna complexes. Interestingly, Chl a/b ratio decreased under low UV-C stress as chlorophyll b accumulated (Fig. 1). Tobacco plants with an enhanced chlorophyll b synthesis have low Chl a/b ratios and accumulate antennal and chloroplastic electron transport proteins, resulting in an enhanced light capture and electron transport rate with positive consequences over the plant total biomass, starch content and light stress tolerance [51]. Therefore, low UV-C dosage might be damaging the photosynthetic antenna complexes but also enhancing the synthesis of chlorophyll b as a photoprotective mechanism working along of also enhanced ROS scavenging and other photoprotective mechanisms. UV-C modulated starch and sugars content in Chlamydomonas as previously observed in crop species [15–17].

The scavenging/stabilizing function of phenolics, sugars and tocopherol are complemented by the activity of also early induced oxidoreductase NDA5 (Additional file 1: Table S1). The Arabidopsis homolog to this protein, NDC1, reduces oxidized plastoglobuli tocopherol and plastoquinone on NADPH. The reduced plastoquinone (PQH_2) into plastoglobuli can easily diffuse back to thylakoidal membranes [46,52] participating in a redox buffering process which can also contribute to ATP synthesis trough the

cycling of electrons around PSI. Thus, PQH_2 would be acting as a central redox balancer which modulates both chloroplastic electron transport rate and chloroplastic ROS scavenging mechanisms.

The enhancement of NDA5 redox modulator under UV-C is complemented by an early increase in carbon fixation, a NADPH consuming process, and the also early efflux of photosynthetic carbon and reducing power from chloroplast. The increase in carbon fixation was supported by the t 5 h accumulation on RBCL and the maintenance of RuBisCO ACTIVASE (RCA1) and RuBisCO SMALL SUBUNIT 2 (RBCS2) levels suggesting an early increase in RuBisCO activity (Additional file 1: Table S1). Interestingly, the differential behavior of the RBCS1 subunit (Additional file 1: Table S1) suggest a possible holoenzyme configuration change under stress. The increase in RuBisCO activity and the early accumulation of glycerol, starch and starch synthesis enzymes support the enhancement on carbon fixation, coupled to its export to the cytoplasm as suggested by the early accumulation of NADPH dependent malate shuttle (MME5) and triose phosphate:Pi (APE2) transporter (Additional file 1: Table S1, S2). RuBisCO upregulation has been described under low UV in microalgae [36]. While NDA5 and carbon fixation can avoid the overreduction of the photosynthetic electron chain at chloroplast level, carbon export would act as a shuttle moving carbon and reducing power in the form of malate and glycerol to and from other cellular compartments [53,54], including the mitochondria, where they can contribute to generate ATP and avoid the overreduction associated to the inhibition of its electron transport chains. (Additional file 1: Table S1). These early redox unbalances would be after the accumulation of subunits associated to the Chlamydomonas CEF supercomplexes (Supplementary Table S1) suggesting the late enhancement of cyclic electron flow under late UV-C acclimation, an ATP producing process. LEF and CEF are independent processes in Chlamydomonas, where supercomplexes of PSI, Cytb6f and FNR are exclusively dedicated to the later and assembly under reducing conditions performing Fd-CEF where FNR consume NADPH to reduce Ferredoxin and contribute to the production of ATP [28,29]. These elements would be part of a larger PSII protection/repair mechanism associated to its uncoupling and the production of needed ATP both for this repair and the avoidance of further damage by ROS. The possible CEF enhancement on UV-C acclimation matched the accumulation of multiple sugars and the phenolic catechin and the fall on early enhanced C3 transport suggesting the recovery of the cell redox balance (Fig. 2, Supplementary Table S1, S2).

Proteome reorganization is a key process to respond to UV-C stress

Proteins are the main target of UV damage, thus, standing under UV radiation require the enhancement of protein turnover mechanisms involving the degradation of damaged proteins, the synthesis of new ones and their fast and coordinated folding and integration into different complexes. PSII is one of the most affected protein complexes under UV with the radiation damaging its central subunits and activating specific responses based on its turnover. The early accumulation of mitochondrial stress chaperone HSP70C subunit, linked to increased mitochondrial protein damage in Chlamydomonas [20], and chloroplastic HSP organizer CDJ1 support a global increase protein damage under UV-C stress. Moreover, the also early accumulation of enzymes involved in amino acid synthesis and the down-accumulation of Ser and Glu, probably funneled towards protein synthesis, supports an enhanced protein turnover

(Additional file 1: Table S1, S2). The activation of the specific PSII turnover response under UV-C was supported by the accumulation of FTSH like protease –FTSHs are associated to damaged PSII under UV stress [47]– central PSII subunits (psbD) and the accumulation of elements related to the correct subunit folding and ensemble as TEF14 and CYN38 (Additional file 1: Table S1).

Either the synthesis of new proteins to substitute damaged, or the modulation of the proteome to acclimate to the new conditions, require a controlled enhancement of protein synthesis which is modulated at translation, transcription, and epigenetic levels. The up-accumulation of translation initiation complex promoters as EIF1A and aminoacyl tRNA synthetases, and the down-accumulation of a possible repressor of this complex (FAP204) under stress suggest a possible balance towards an enhanced translation activity under the tested stress (Additional file 1: Table S1). FAP204 was defined as a possible repressor as its human homolog, OLA1, inhibits translation initiation complex formation [55]. Interestingly the three translation related elements were clustered in the protein interaction networks suggesting a common regulation (Fig. 5, Additional file 2: Figure S2). The changes in translational activity are always a reflex of prior transcriptional and epigenetic changes, thus same changes could be happening under UV-C stress. Epigenetic changes were represented by the early depletion of the histone demethylase JMJC DOMAIN CONTAINING PROTEIN 7 and the histone methyltransferase PRMT2 (Additional file 1: Table S1). Arabidopsis homologs to these, JMJ32 and PRMT10, are linked to environment based FLC modulation [56,57]. Thus, their depletion in the microalgae would be related to the epigenetic control of stress response genes under UV-C. Ultimately, transcription linked epigenetic modulation with the observed changes in translational activity. Multiple RNA processing proteins accumulated under stress and interestingly some of these were linked in the sPLS-STRING network to the early accumulated and redox/energy metabolism-related glycerol which might have a signaling function (Fig. 5; Additional file 1: Table S1, S2).

Novel signalers are involved in the UV-C induced modulation of Chlamydomonas metabolism

The early response of Chlamydomonas to the UV-C irradiation was mainly based on protein protection and redox modulation to limit further direct UV and ROS damage. This response was probably coupled to ROS-based signaling pathways as in land plants [4,58], although no evidences were found of the involvement of salicylic and jasmonic acids, common plant ROS signalers upregulated in UV-C stressed plants [3].

Regardless of the still unknown microalgae UV-C perception and signaling mechanisms the omic and systems biology approach to this stress linked many proteins and metabolites, some of them previously unidentified as CPLD58 and the novel FTSH protease, to the observed UV-C effect over Chlamydomonas photosynthesis, protein turnover, biomass and cell proliferation (Fig. 1a, b). The translation modulator FAP204 and the cell proliferation related PP2A like and MINA53 proteins are also examples of previously unidentified proteins which could be respectively associated to the enhanced protein turnover under UV-C and to the modulation of the culture growth, which was transiently reduced 5 h after stress imposition. On the other hand, the acclimation accumulated an also previously unidentified DYRK kinase was associated

in the sPLS-STRING network to the late accumulated sugar (UNKNOWN SUGAR 5) pointing to their role in the observed modulation of biomass composition under UV-C (Fig. 5). Interestingly, other DYRK kinases modulate starch and oil accumulation in stressed Chlamydomonas [45]. All these elements –related to translation, transcription and epigenetic mechanisms– have been identified as promising targets for the further characterization of the UV-C response or the exploitation of the UV metabolic modulation mechanisms towards the engineering of more productive strains.

Conclusion

Chlamydomonas response to UV-C stress is based on the avoidance of protein damage requiring globally from the enhancement of protein protection/turnover and ROS scavenging and the modulation of photosynthesis and redox. The Chlamydomonas early response to UV-C irradiation is mainly based on protein turnover/protection, singlet oxygen focused ROS scavenging and metabolic/redox modulation through the enhancement of carbon and reducing power exchange between cellular compartments. This fast response is coupled to probably ROS-and macromolecule damage-mediated signaling that would be driving a fine UV-tuned control of cell proliferation, gene expression and protein translation before Chlamydomonas late and more complex acclimation responses. Acclimation was related to specific proteome changes focused on the photosystems modulation, uncoupling PSII, enhancing CEF the modulation of antenna size, and the accumulation of probably ROS scavenging sugars and starch. Some of the found early and previously unknown response signalers as translation modulator FAP204, cell proliferation related PP2A like protein and MINA53, and late acclimation metabolic modulator DYRK have been identified as promising targets for the further characterization of the UV-C microalgae response, including the modulation of the biomass content. Similarities between the sugar focused UV-C response of Chlamydomonas, and those previously described in crop species make this work applicable to improvement strategies aimed at a broad range of species as plants and microalgae.

Methods

Strains and Cultures

Chlamydomonas reinhardtii CC-503 cw92 cultures were grown on a culture chamber (25 °C, 120 rpm, continuous 85 µE m^2 s^{-1} irradiance provided by Sylvania GroLux lamps) in HEPES Acetate Phosphate (HAP) culture media [59]. HAP was formulated from Tris Acetate Phosphate (TAP) [60], substituting Tris for HEPES as a Mass Spectrometry (MS) compatible buffer. To induce UV stress, cultures were irradiated with a low UV-C dose of 0.1 $W{\cdot}m^{-2}$ during the first 15 minutes upon experiment start. UV-C was provided by PHILIPS TUV 36W/G36 T8 lamps with a discrete UV-C emission peak at 250 nm. Initial culture was prepared 48 h before experiment start diluting twentyfold a seed culture originated from a single colony. After 48 h, cells were harvested and diluted to $5{\cdot}10^5$ cell/mL splitting the resulting culture volume between nine flasks.

Physiological Measurements

Three flasks were sampled on each harvesting time, placed at the experiment start (0 h) and after 5 and 24 h of UV exposition (Fig. 6). Cell density was measured on each harvesting time by measuring the culture absorbance at 630 and 750 nm using the Nabi UV/vis Nano Spectrophotometer (MicroDigital Co., Korea) and the cultures photosynthetic rate (Fv/Fm) was measured with an imaging/pulse-amplitude modulation fluorimeter (OS1-FL, Opti-Sciences). Parallelly, 150 mL of culture were taken from each harvested flask and divided in three 50 mL aliquots which were centrifuged at 4000 x g. Pellets fresh weight (FW) was calculated gravimetrically and then immediately frozen in liquid nitrogen. One of the three pellets harvested from each flask was employed for the combined extraction of metabolites and proteins, according to Valledor, *et al.* (2014) [61]. The second pellet was employed for the quantification of pigments (Chlorophyll a, b and carotenoids) according to Sims and Gamon (2002) [62]. Starch, soluble sugars, free aminoacids, lipid peroxidation and phenolic compounds were measured from the remaining pellet using a novel colorimetric protocol López-Hidalgo, C (unpublished) using the Nabi UV/vis Nano Spectrophotometer (MicroDigital Co., Korea). Briefly, this protocol starts from a single Chlamydomonas extract resulting from the homogenization of the cell pellet in ethanol 80%. Aliquots from this extract were employed in different ethanol-based colorimetric protocols derived from the combination and modification of previous methods for the quantification of starch and soluble sugars [63,64], free amino acids [65], phenolic compounds [66] and the lipid peroxidation product MDA [67].

Bengal rose drop assay

Two milliliters samples taken from each harvested flask were adjusted to $5{\cdot}10^5$ cell/mL and divided in two 1 mL aliquots. 2 µM rose bengal (RB) (Merck, Germany) was added to one of the aliquots into each pair. Resulting RB containing and control aliquots were challenged during 30 minutes under constant light and then three drops of 3 µL from each one were plated onto a HAP agar plate and maintained under constant light for 48 h.

Quantitative Proteome Analysis (GeLC-LTQ-Orbitrap MS)

The preparation of protein samples for MS/MS analysis was performed following Valledor, *et al.* (2014) [68] recommendations. Ten micrograms of trypsin digested peptides were loaded per injection into a one-dimensional nano-flow LC-Orbitrap/MS and resolved in a 90-min gradient from 5 to 40% (v/v) acetonitrile/0.1% (v/v) formic acid using a monolithic C18 column (Chromolith RP-18r, Merck, Darmstadt, Germany). MS analysis was performed on an Orbitrap LTQ XL mass spectrometer [59].

Raw data coming from Orbitrap was searched with Proteome Discoverer version 2.1 (Thermo) SEQUEST algorithm as previously described [69], employing a label-free quantification based on precursor's areas. Chlamydomonas 5.5 protein (18750 accessions), Chlamydomonas chloroplast & mitochondria (84 accessions) and Swissprot-viridiplantae (36097 accessions) databases were employed for protein identification. Only high confidence proteins (at least one significant peptide, XCorr > 1.8, FDR 5%) present in all the biological samples of at least one treatment were considered for this analysis.

Metabolite GC-MS Analysis

Polar fraction analysis were carried out following Valledor, *et al.* (2014) [68] protocol with some minor changes on a triple quad instrument (TSQ Quantum GC; Thermo). In brief, 1 µL of sample was injected, and GC separated into a HP-5MS capillary column (30 m 0.25 mm) (Agilent Technologies). Oven temperature was increased from 80 °C to 200 °C at a 3 °C per min rate and then reduced to 25 °C at 10 °C per min and maintained at 25 °C for 3 min, followed by 4 min of post run conditions at 30 °C. Mass spectrometer was operated in electron impact (EI) mode at 70 eV in a scan range of m/z 40–600. The identification of metabolites was based on the spectral characteristics and GC retention times of each individual metabolite through its comparison with the retention times and spectral characteristics of standards available in our in-house library and in Golm Metabolome Database [70].

Biostatistical analyses

R v3.3 (R Core Team, 2019) software core functions and pRocessomics package (available at https://github.com/Valledor/pRocessomics) were used for all performed statistical procedures.

Proteomics and metabolomics datasets missing values were imputed through a sequential K-Nearest Neighbor algorithm. Imputation was performed only when one value per sampling point was missing. Protein and metabolite abundances were re-estimated afterwards following a sample-centric approach (individual peak areas divided by total peak area per sample). Data was then subjected to univariate (one-way ANOVA 0.05, 5% FDR for protein variables, followed by a Tukey HSD post-hoc test in all cases) and multivariate analyses: Principal Component Analysis (PCA), Heatmap clustering and sparse Partial Least Squares regression analysis (sPLS).

sPLS-based multivariate models [72] were employed after a tuning process selecting the best combination of protein and metabolite variables to build correlation networks employing the R package mixOmics [73] using proteins as predictors and metabolites as response. Resulting correlation network was filtered keeping edges with correlation values above 0.6. Correlation network nodes were used as input to build known protein-protein and protein-protein/protein-metabolite interaction networks into the STRING and STITCH platforms respectively [74]. Resulting networks were visualized and processed in Cytoscape V3.6.1 [75], including the overlapping of the sPLS and STRING networks. Cytoscape plug in StringApp [76] was used for STRING and STICH network import, setting interaction confidence to 0.4 (medium confidence).

Abbreviations

abscisic acid	ABA
Cyclic Electron Flow	CEF
HEPES Acetate Phosphate	HAP
jasmonates	JA
Linear Electron Flow	LEF
Photosystem I	PSI
Photosystem II	PSII
Principal Component 1	PC1
Principal Component 2	PC2
Principal Component Analysis	PCA
Reactive Oxygen Species	ROS
reduced plastoquinone	PQH2
salicylic acid	SA
sparse Partial Least Squares regression analysis	sPLS
triacylglycerols	TAG
Tris Acetate Phosphate	TAP
Oxygen Evolving Complex	OEC

Declarations

Ethics approval and consent to participate

Not applicable.

Consent for publication

Not applicable.

Availability of data and materials

The datasets used and/or analyzed during the current study are available from the corresponding author on reasonable request. The Chlamydomonas JGI v5.5, Viridiplantae-UniProt or Augustus database accessions for all proteins referred in the manuscript are available in the Additional file 1: Table S1 and Table 1. Golm database identifiers for all metabolites referred in the manuscript are available at Additional file 1: Table S2.

Competing interests

The authors declare that they have no competing interests.

Funding

This work was supported by the AGL2016-77633-P and AGL2017-83988-R (Spanish Ministry of Science, Innovation and University). FC, MC, LV and MM were generously granted by the BP14-138 and BP19-137 (Programa de Ayudas Predoctorales Severo Ochoa, Autonomous Community of Asturias, Spain; to FC and MC), RYC-2015-17871 and RYC-2014-14981 (Ramón y Cajal Programme, Spanish Ministry of Economy and Competitiveness; to LV and MM) fellowships respectively.

Authors' contributions

LV, MM and MJC conceived this study; FC, MC MM and LV performed research, analyzed the data and wrote the manuscript. All authors read and approved the final manuscript.

Acknowledgements

We thank L. García Campa and C. López Hidalgo for their valuable discussions and advices and anonymous reviewers for their helpful comments.

References

1. Tilbrook K, Dubois M, Crocco CD, Yin R, Chappuis R, Allorent G, et al. UV-B Perception and Acclimation in Chlamydomonas reinhardtii. Plant Cell. 2016;
2. Liang T, Yang Y, Liu H. Signal transduction mediated by the plant UV-B photoreceptor UVR8. New Phytol. 2018.
3. Takeno K. Stress-induced flowering: The third category of flowering response. J. Exp. Bot. 2016.
4. Xu Y, Charles MT, Luo Z, Mimee B, Tong Z, Véronneau PY, et al. Ultraviolet-C priming of strawberry leaves against subsequent Mycosphaerella fragariae infection involves the action of reactive oxygen species, plant hormones, and terpenes. Plant Cell Environ. 2019;
5. Sharma K, Li Y, Schenk PM. UV-C-mediated lipid induction and settling, a step change towards economical microalgal biodiesel production. Green Chem. 2014;
6. Sharma KK, Ahmed F, Schenk PM, Li Y. UV-C mediated rapidcarotenoid induction and settling performance of Dunaliellasalina and Haematococcus pluvialis. Biotechnol Bioeng. 2015;
7. Ahmed F, Schenk PM. UV–C radiation increases sterol production in the microalga Pavlova lutheri. Phytochemistry. 2017;
8. Urban L, Charles F, de Miranda MRA, Aarrouf J. Understanding the physiological effects of UV-C light and exploiting its agronomic potential before and after harvest. Plant Physiol. Biochem. 2016.

9. Christie JM, Arvai AS, Baxter KJ, Heilmann M, Pratt AJ, Hara AO, et al. Plant UVR8 Photoreceptor Senses Disruption of Cross-Dimer Salt Bridges. Science (80-). 2012;335:1492–7.
10. Velanis CN, Herzyk P, Jenkins GI. Regulation of transcription by the Arabidopsis UVR8 photoreceptor involves a specific histone modification. Plant Mol Biol. 2016;92:425–43.
11. Müller-Xing R, Xing Q, Goodrich J. Footprints of the sun: memory of UV and light stress in plants. Front Plant Sci [Internet]. 2014;5. Available from: http://journal.frontiersin.org/article/10.3389/fpls.2014.00474/abstract
12. Xu Y, Charles MT, Luo Z, Mimee B, Veronneau PY, Rolland D, et al. Preharvest Ultraviolet C Irradiation Increased the Level of Polyphenol Accumulation and Flavonoid Pathway Gene Expression in Strawberry Fruit. J Agric Food Chem. 2017;65:9970–9.
13. Tian J, Yu J. Changes in ultrastructure and responses of antioxidant systems of algae (…. J Photochem Photobiol. 2009;
14. Forján E, Garbayo I, Henriques M, Rocha J, Vega JM, Vílchez C. UV-A Mediated Modulation of Photosynthetic Efficiency, Xanthophyll Cycle and Fatty Acid Production of Nannochloropsis. Mar Biotechnol. 2011;
15. Bornman JF, Evert RF, Mierzwa RJ. The effect of UV-B and UV-C radiation on sugar beet leaves. Protoplasma. 1983;
16. Lin Q, Xie Y, Liu W, Zhang J, Cheng S, Xie X, et al. UV-C treatment on physiological response of potato (Solanum tuberosum L.) during low temperature storage. J Food Sci Technol. 2017;
17. Huang H, Ge Z, Limwachiranon J, Li L, Li W, Luo Z. UV-C treatment affects browning and starch metabolism of minimally processed lily bulb. Postharvest Biol Technol. 2017;
18. Schwacke R, Ponce-Soto GY, Krause K, Bolger AM, Arsova B, Hallab A, et al. MapMan4: A Refined Protein Classification and Annotation Framework Applicable to Multi-Omics Data Analysis. Mol Plant [Internet]. 2019;12:879–92. Available from: http://www.sciencedirect.com/science/article/pii/S1674205219300085
19. Bottinger L, Guiard B, Oeljeklaus S, Kulawiak B, Zufall N, Wiedemann N, et al. A complex of Cox4 and mitochondrial Hsp70 plays an important role in the assembly of the cytochrome c oxidase. Mol Biol Cell [Internet]. 2013;24:2609–19. Available from: http://www.molbiolcell.org/cgi/doi/10.1091/mbc.E13-02-0106
20. Schroda M, Hemme D, Mühlhaus T. The Chlamydomonas heat stress response. Plant J [Internet]. 2015;n/a-n/a. Available from: http://doi.wiley.com/10.1111/tpj.12816
21. Hirano G, Izumi H, Yasuniwa Y, Shimajiri S, Ke-Yong W, Sasagiri Y, et al. Involvement of riboflavin kinase expression in cellular sensitivity against cisplatin. Int J Oncol. 2011;38:893–902.
22. Cazzaniga S, Kim M, Bellamoli F, Jeong J, Lee S, Perozeni F, et al. Photosystem II antenna complexes CP26 and CP29 are essential for nonphotochemical quenching in Chlamydomonas reinhardtii. Plant Cell Environ. 2020;
23. Viczián A, Máté Z, Nagy F, Vass I. UV-b induced differential transcription of psbD genes encoding the D2 protein of Photosystem II in the cyanobacterium Synechocystis 6803. Photosynth Res.

2000;64:257–66.

24. Fu A, He Z, Cho HS, Lima A, Buchanan BB, Luan S. A chloroplast cyclophilin functions in the assembly and maintenance of photosystem II in Arabidopsis thaliana. Proc Natl Acad Sci [Internet]. 2007;104:15947–52. Available from: http://www.pnas.org/cgi/doi/10.1073/pnas.0707851104
25. de Bianchi S, Betterle N, Kouril R, Cazzaniga S, Boekema E, Bassi R, et al. Arabidopsis Mutants Deleted in the Light-Harvesting Protein Lhcb4 Have a Disrupted Photosystem II Macrostructure and Are Defective in Photoprotection. Plant Cell [Internet]. 2011;23:2659–79. Available from: http://www.plantcell.org/cgi/doi/10.1105/tpc.111.087320
26. Liu J, Last RL. A chloroplast thylakoid lumen protein is required for proper photosynthetic acclimation of plants under fluctuating light environments. Proc Natl Acad Sci [Internet]. 2017;201712206. Available from: http://www.pnas.org/lookup/doi/10.1073/pnas.1712206114
27. Willmund F, Dorn K V, Schulz-Raffelt M, Schroda M. The Chloroplast DnaJ Homolog CDJ1 of Chlamydomonas reinhardtii Is Part of a Multichaperone Complex Containing HSP70B, CGE1, and HSP90C. PLANT Physiol [Internet]. 2008;148:2070–82. Available from: http://www.plantphysiol.org/cgi/doi/10.1104/pp.108.127944
28. Iwai M, Takizawa K, Tokutsu R, Okamuro A, Takahashi Y, Minagawa J. Isolation of the elusive supercomplex that drives cyclic electron flow in photosynthesis. Nature. 2010;
29. Takahashi H, Clowez S, Wollman FA, Vallon O, Rappaport F. Cyclic electron flow is redox-controlled but independent of state transition. Nat Commun. 2013;
30. Carrie C, Murcha MW, Kuehn K, Duncan O, Barthet M, Smith PM, et al. Type II NAD(P)H dehydrogenases are targeted to mitochondria and chloroplasts or peroxisomes in Arabidopsis thaliana. FEBS Lett. 2008;582:3073–9.
31. Fatihi A, Latimer S, Schmollinger S, Block A, Dussault PH, Vermaas WFJ, et al. A Dedicated Type II NADPH Dehydrogenase Performs the Penultimate Step in the Biosynthesis of Vitamin K_1 in S*ynechocystis* and Arabidopsis. Plant Cell. 2015;27:1730–41.
32. Hideg É, Barta C, Kálai T, Vass I, Hideg K, Asada K. Detection of singlet oxygen and superoxide with fluorescent sensors in leaves under stress by photoinhibition or UV radiation. Plant Cell Physiol. 2002;
33. Ledford HK, Chin BL, Niyogi KK. Acclimation to singlet oxygen stress in Chlamydomonas reinhardtii. Eukaryot Cell. 2007;
34. Li D, Luo Z, Mou W, Wang Y, Ying T, Mao L. ABA and UV-C effects on quality, antioxidant capacity and anthocyanin contents of strawberry fruit (Fragaria ananassa Duch.). Postharvest Biol Technol. 2014;
35. Corpas FJ, Barroso JB. NADPH-generating dehydrogenases: Their role in the mechanism of protection against nitro-oxidative stress induced by adverse environmental conditions. Front Environ Sci. 2014;
36. Zhang X, Tang X, Zhou B, Hu S, Wang Y. Effect of enhanced UV-B radiation on photosynthetic characteristics of marine microalgae Dunaliella salina (Chlorophyta, Chlorophyceae). J. Exp. Mar. Bio. Ecol. 2015. p. 27–35.

37. Tsai AYL, Gazzarrini S. Trehalose-6-phosphate and SnRK1 kinases in plant development and signaling: The emerging picture. Front. Plant Sci. 2014.
38. Wurzinger B, Mair A, Fischer-Schrader K, Nukarinen E, Roustan V, Weckwerth W, et al. Redox state-dependent modulation of plant SnRK1 kinase activity differs from AMPK regulation in animals. FEBS Lett. 2017.
39. Xuan F, Huang M, Zhao E, Cui H. MINA53 deficiency leads to glioblastoma cell apoptosis via inducing DNA replication stress and diminishing DNA damage response. Cell Death Dis. 2018;9.
40. Durian G, Rahikainen M, Alegre S, Brosché M, Kangasjärvi S. Protein Phosphatase 2A in the Regulatory Network Underlying Biotic Stress Resistance in Plants. Front Plant Sci [Internet]. 2016;7. Available from: http://journal.frontiersin.org/Article/10.3389/fpls.2016.00812/abstract
41. Punzo P, Ruggiero A, Possenti M, Nurcato R, Costa A, Morelli G, et al. The PP2A-interactor TIP41 modulates ABA responses in Arabidopsis thaliana. Plant J. 2018;94:991–1009.
42. Tang S, Qin F, Wang X, Liang Z, Cai H, Mo L, et al. H2O2induces PP2A demethylation to downregulate mTORC1 signaling in HEK293 cells. Cell Biol Int. 2018;42:1182–91.
43. Zheng Y, Jiao C, Sun H, Rosli HG, Pombo MA, Zhang P, et al. iTAK: A Program for Genome-wide Prediction and Classification of Plant Transcription Factors, Transcriptional Regulators, and Protein Kinases. Mol Plant [Internet]. 2016;9:1667–70. Available from: http://www.sciencedirect.com/science/article/pii/S1674205216302234
44. Kajikawa M, Sawaragi Y, Shinkawa H, Yamano T, Ando A, Kato M, et al. Algal Dual-Specificity Tyrosine Phosphorylation-Regulated Kinase, Triacylglycerol Accumulation Regulator1, Regulates Accumulation of Triacylglycerol in Nitrogen or Sulfur Deficiency. Plant Physiol [Internet]. 2015;168:752–64. Available from: http://www.plantphysiol.org/lookup/doi/10.1104/pp.15.00319
45. Schulz-Raffelt M, Chochois V, Auroy P, Cuiné S, Billon E, Dauvillée D, et al. Hyper-accumulation of starch and oil in a Chlamydomonas mutant affected in a plant-specific DYRK kinase. Biotechnol Biofuels. 2016;9.
46. Eugeni Piller L. Role of plastoglobules in metabolite repair in the tocopherol redox cycle. Front Plant Sci. 2014;5.
47. Pascual J, Cañal MJ, Escandón M, Meijón M, Weckwerth W, Valledor L. Integrated Physiological, Proteomic, and Metabolomic Analysis of Ultra Violet (UV) Stress Responses and Adaptation Mechanisms in *Pinus radiata*. Mol Cell Proteomics. 2017;
48. Sami F, Yusuf M, Faizan M, Faraz A, Hayat S. Role of sugars under abiotic stress. Plant Physiol Biochem [Internet]. 2016;109:54–61. Available from: http://www.sciencedirect.com/science/article/pii/S0981942816303552
49. Escandón M, Cañal MJ, Pascual J, Pinto G, Correia B, Amaral J, et al. Integrated physiological and hormonal profile of heat-induced thermotolerance in Pinus radiata. Tree Physiol. 2015;
50. Valentin HE, Lincoln K, Moshiri F, Jensen PK, Qi Q, Venkatesh T V, et al. The Arabidopsis vitamin E pathway gene5-1 mutant reveals a critical role for phytol kinase in seed tocopherol biosynthesis.

Plant Cell [Internet]. American Society of Plant Biologists; 2006;18:212–24. Available from: https://www.ncbi.nlm.nih.gov/pubmed/16361393

51. Biswal AK, Pattanayak GK, Pandey SS, Leelavathi S, Reddy VS, Govindjee, et al. Light intensity-dependent modulation of chlorophyll b biosynthesis and photosynthesis by overexpression of chlorophyllide a oxygenase in tobacco. Plant Physiol. 2012;
52. Eugeni Piller L, Besagni C, Ksas B, Rumeau D, Bréhélin C, Glauser G, et al. Chloroplast lipid droplet type II NAD(P)H quinone oxidoreductase is essential for prenylquinone metabolism and vitamin K₁ accumulation. Proc Natl Acad Sci. 2011;108:14354 LP – 14359.
53. Davis MC, Fiehn O, Durnford DG. Metabolic acclimation to excess light intensity in Chlamydomonas reinhardtii. Plant Cell Environ [Internet]. 2013;36:1391–405. Available from: https://onlinelibrary.wiley.com/doi/abs/10.1111/pce.12071
54. Demmig-Adams B, Burch TA, Stewart JJ, Savage EL, Adams WW. Algal glycerol accumulation and release as a sink for photosynthetic electron transport. Algal Res [Internet]. 2017;21:161–8. Available from: http://www.sciencedirect.com/science/article/pii/S2211926416306762
55. Chen H, Song R, Wang G, Ding Z, Yang C, Zhang J, et al. OLA1 regulates protein synthesis and integrated stress response by inhibiting eIF2 ternary complex formation. Sci Rep. 2015;5.
56. Gan ES, Xu Y, Wong JY, Geraldine Goh J, Sun B, Wee WY, et al. Jumonji demethylases moderate precocious flowering at elevated temperature via regulation of FLC in Arabidopsis. Nat Commun. 2014;5.
57. Niu L, Lu F, Pei Y, Liu C, Cao X. Regulation of flowering time by the protein arginine methyltransferase AtPRMT10. EMBO Rep. 2007;8:1190–5.
58. Lee JE, Cho YU, Kim KH, Lee DY. Distinctive metabolomic responses of Chlamydomonas reinhardtii to the chemical elicitation by methyl jasmonate and salicylic acid. Process Biochem. 2016;51:1147–54.
59. Valledor L, Furuhashi T, Hanak AM, Weckwerth W. Systemic cold stress adaptation of chlamydomonas reinhardtIII. Mol Cell Proteomics. 2013;
60. Harris EH. The Chlamydomonas Sourcebook: Introduction to Chlamydomonas and Its Laboratory Use. UK: Academic Press, Oxford, UK; 2009.
61. Valledor L, Escandón M, Meijón M, Nukarinen E, Cañal MJ, Weckwerth W. A universal protocol for the combined isolation of metabolites, DNA, long RNAs, small RNAs, and proteins from plants and microorganisms. Plant J. 2014;
62. Sims DA, Gamon JA. Relationships between leaf pigment content and spectral reflectance across a wide range of species, leaf structures and developmental stages. Remote Sens Environ [Internet]. Elsevier; 2002;81:337–54. Available from: http://www.sciencedirect.com/science/article/pii/S003442570200010X
63. Chow PS, Landhäusser SM. A method for routine measurements of total sugar and starch content in woody plant tissues. Tree Physiol. 2004;

64. Haldar D, Sen D, Gayen K. Development of Spectrophotometric Method for the Analysis of Multi-component Carbohydrate Mixture of Different Moieties. Appl Biochem Biotechnol. 2017;
65. MOORE S, STEIN WH. A modified ninhydrin reagent for the photometric determination of amino acids and related compounds. J Biol Chem. 1954;
66. Ainsworth EA, Gillespie KM. Estimation of total phenolic content and other oxidation substrates in plant tissues using Folin-Ciocalteu reagent. Nat Protoc. 2007;
67. Hodges DM, DeLong JM, Forney CF, Prange RK. Improving the thiobarbituric acid-reactive-substances assay for estimating lipid peroxidation in plant tissues containing anthocyanin and other interfering compounds. Planta. 1999;
68. Valledor L, Furuhashi T, Recuenco-Muñoz L, Wienkoop S, Weckwerth W. System-level network analysis of nitrogen starvation and recovery in Chlamydomonas reinhardtii reveals potential new targets for increased lipid accumulation. Biotechnol Biofuels. 2014;7.
69. Valledor L, Recuenco-Munoz L, Egelhofer V, Wienkoop S, Weckwerth W. The different proteomes of Chlamydomonas reinhardtii. J Proteomics. 2012;75.
70. Fernie AR, Usadel B, Birkemeyer C, Steinhauser D, Bergmüller E, Kopka J, et al. GMD@CSB.DB: the Golm Metabolome Database. Bioinformatics [Internet]. 2004;21:1635–8. Available from: https://doi.org/10.1093/bioinformatics/bti236
71. R Core Team. R: A Language and Environment for Statistical Computing [Internet]. Vienna, Austria; 2019. Available from: https://www.r-project.org
72. Le Cao K-A, Rossow D, Robert-Granié C, Besse P. A Sparse PLS for Variable Selection when Integrating Omics data. Stat Appl Genet Mol Biol. 2008;7:35.
73. Lê Cao K-AK-A, González I, Déjean S, González I. Unravelling “omics” data with the R package mixOmics. HAL. 2012;
74. Szklarczyk D, Santos A, von Mering C, Jensen LJ, Bork P, Kuhn M. STITCH 5: augmenting protein-chemical interaction networks with tissue and affinity data. Nucleic Acids Res [Internet]. 2015/11/20. Oxford University Press; 2016;44:D380–4. Available from: https://www.ncbi.nlm.nih.gov/pubmed/26590256
75. Shannon P, Markiel A, Owen Ozier 2, Baliga NS, Wang JT, Ramage D, et al. Cytoscape: a software environment for integrated models of biomolecular interaction networks. Genome Res. 2003;2498–504.
76. Doncheva NT, Morris JH, Gorodkin J, Jensen LJ. Cytoscape StringApp: Network Analysis and Visualization of Proteomics Data. J Proteome Res. United States; 2019;18:623–32.

Additional Files

Additional file 1 (Additional file 1. xls)

Additional file 1: Table S1: List of the 885 quantified proteins in whole cell fractions with their abundances estimated following a NSAF approach. Protein are designated with their respective

Chlamydomonas JGI v5.5, Viridiplantae-UniProt or Augustus database accession. Percent of coverage, number of unique peptides used for identification, residues and protein molecular weight are indicated. Displayed data underwent filtering, imputation and sample abundance-based balancing. The mean abudance ± SD for each sampling time is indicated as well as their ANOVA p- and q-values (BH), and the post-hoc Tukey HSD test p-values calculated over Log10 transformed data. Deflines, symbols and MapMan bins were manually curated. **Table S2:** List of the 68 quantified metabolites. Metabolite names were included along their Golm metabolome database identifiers used as the main names of uncharacterized compounds. Retention time (RT) was included along the mass/charge ratios (M/Z 1 and MZ 2) of the two most characteristic fragmentation ions for each compound. Metabolite abundance was estimated from the peak areas of the indicated characteristic ions. Abundance data underwent filtering, imputation and sample abundance-based balancing. The mean abundance respect to control ± SD for each sampling time are indicated as well as ANOVA p–values and post-hoc Tukey (HSD) test p-values calculated over z-centered data. MapMan bins and deflines were manually curated. **Table S3.** Physiological parameters related to photosynthesis –chlorophyll a (Chl a), chlorophyll b (Chl b), carotenoids (Car), total chlorophyll content (Chl a+b), and Fv/Fm and Chl a/b ratios–, culture total biomass –average cell density (cell/mL) and fresh weight per mL of culture (FW)–, biomass composition –Lipid weight (LW), starch, soluble sugars, free aminoacids and phenolics abundance– and oxidative stress-related malondialdehyde (MDA) content. Pigment (Chl a, Chl b, Car), biomass composition measures (LW, starch, free aminoacids, soluble sugars and phenolics) and MDA abundance were expressed as µmol, mg and nmol per mg of FW respectively. For each parameter is represented the harvesting time mean and SD. Significative differences were detected trough a one-way ANOVA (α=0.05) over z-centered data. Tukey HSD post-hoc test (α=0.05) was performed in order define diferences between the different harvesting times. **Table S4:** Summary of z-score transformed protein abundance PCA. Scores of the nine generated components for each sample are showed along proportion of the total sample variance explained by each component and loadings relating each protein variable contribution to each generated component. Proteins were identified by their respective Phytozome v5.5, Viridiplantae-UniProt or Augustus identifier. **Table S5:** Summary of z-score transformed metabolite abundance PCA. Scores of the nine generated components for each sample are showed along proportion of the total sample variance explained by each component and loadings relating each metabolite variable contribution to each generated component. Metabolites were identified by their respective names or their Golm metabolome database identifiers for those uncharacterized ones. **Table S6:** Summary of z-score transformed protein and metabolite abundance sPLS. Model was tuned keeping 125 protein (X) and 9 metabolite/physiology (Y) variables. Loadings relating each keep protein (X) or metabolite and physiological variables (Y) contribution to each two generated components are listed along the variable identifiers Proteins were identified by their respective Phytozome v5.5, UNIPROT-Viridiplantae or Augustus identifier. Metabolites were identified by their respective name or for uncharacterized compounds their Golm database identifier.

Additional file 2 (Additional file 2. pdf)

Additional file 2: Figure S1. PCA biplots over z-score transformed data from protein (A) and metabolite (B) showing divergence between samples from different harvesting times and the correlation of each individual variables to each displayed component. Protein PCA (A) principal component 1 (PC1) potentially gathers variability related to the photoacclimation to UV-B/C with photosynthesis PHOTOSYSTEM II D2 PROTEIN (psbD) and CHLOROPHYLL A-B BINDING PROTEIN (LHCB4) as some of its highest rank elements. Principal component 2 (PC2) collects early response elements with signaling. WD40 REPEAT PROTEIN (Cre12.g495650.t1.2), carbon metabolism an redox-related NADP MALIC ENZYME 5 (MME5) and TYPE II NADH DEHYDROGENASE (NDA5) and protein damage-associated HEAT SHOCK PROTEIN 70C, E (HSP70C, HSP70E) had the highest loadings within this component. At metabolome level (B), PC1 explain early response with phenolic metabolism protocatechuic and 4-hydroxybenzoic acids; while PC2 joins late accumulated sugars and UV shielding catechin, both related to acclimation. Bigger dots represent individual samples and were colored according to their harvesting time (0, 5, 24 h), while small dots represent individual variables and were colored according to their MapMan category. **Figure S2.** sPLS based STITCH network. STITCH network nodes were colored according to their MapMan categories and shaped according to the omic level element they represented (circle for proteins, quadrangle for metabolites). Edge color was link to interaction confidence (STITCH interaction score). Confidence threshold was set at 0.4 (medium confidence). Network highlighted C3 derived glycerol redox valve central role under UV-C, between protein biosynthesis, respiration modulation, lipid metabolism and oxidative stress response. Same network connected translation related EIF1a, PP2A like (Cre03.g199983.t1.1) and FAP204 to C/N metabolism and translation modulation. Translation/development related MINA53 was also connected in this network to unknown WD40 repeat protein.

Figures

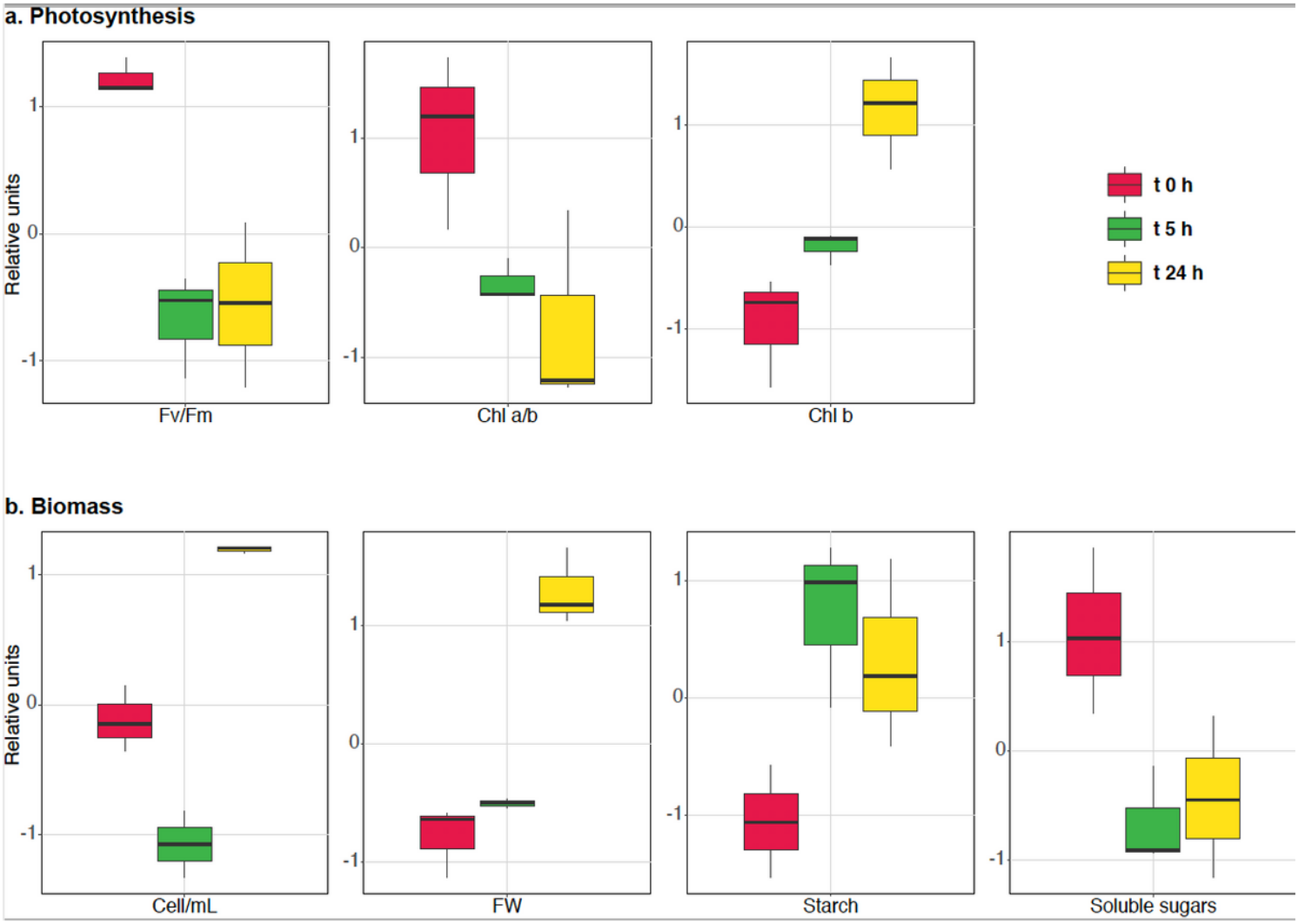

Figure 1

Box plot graphs showing the physiological and structural changes on Chlamydomonas cells exposed to a low UV-C dosage. Significative changes (ANOVA □ 0.05) in culture photosynthetic parameters including Chl b abundance, and Fv/Fm and Chl a/b ratios (a). UV-C effects on culture cellular density (Cell/mL) and culture biomass as average fresh weight per mL of culture (FW) (b).

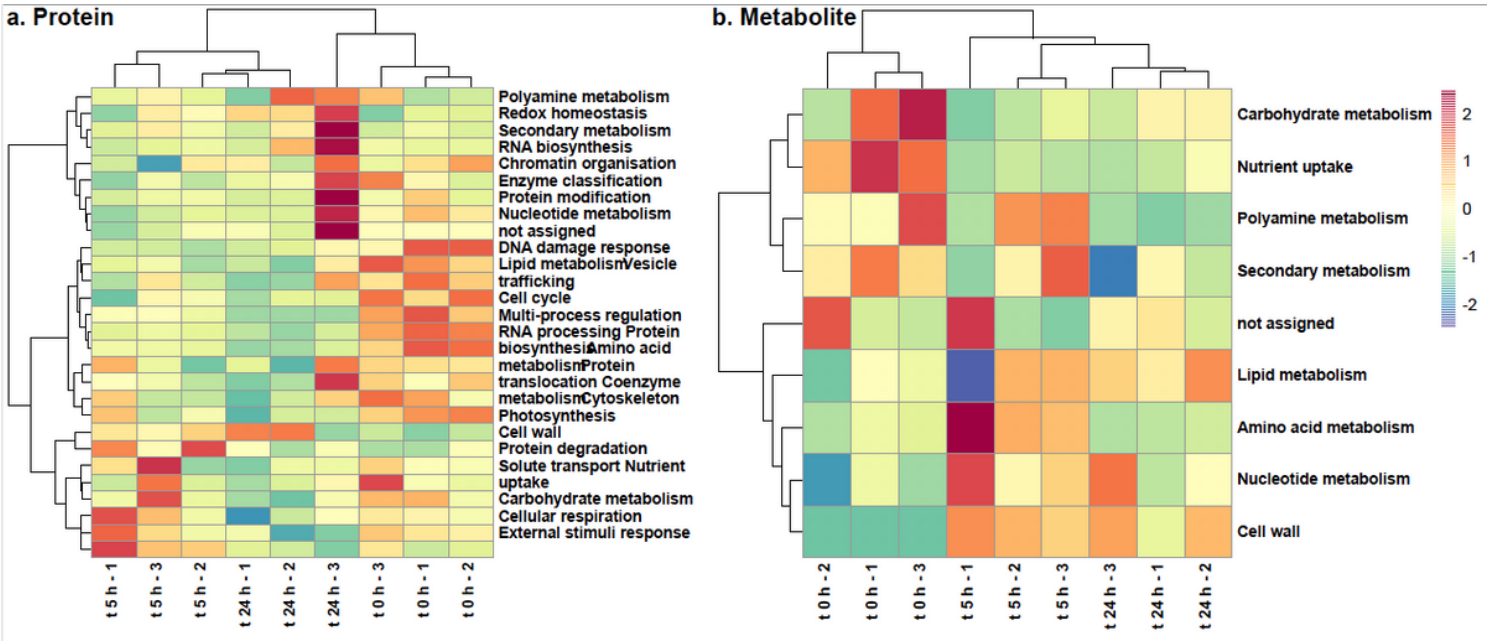

Figure 2

Heatmap biclustering plots over MapMan categories protein (a) or metabolite (b) total abundance. Tree was built based on Manhattan distances and Ward aggregation method. Samples clustered according to their harvesting time and differences in abundance were observed between harvesting times for some functional categories into both plots.

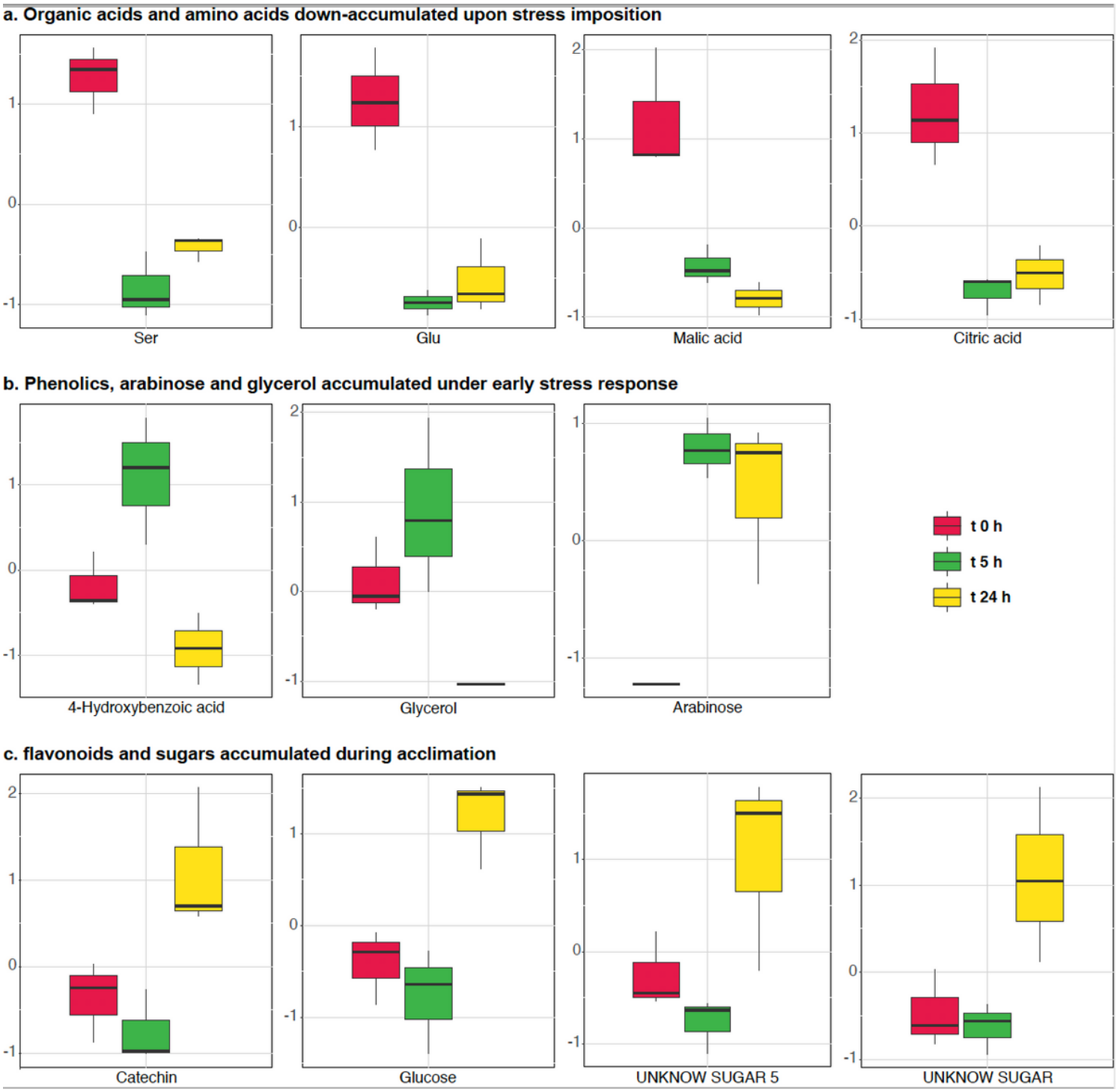

Figure 3

Box plot graphs representing the abundance change of the differentially accumulated metabolites on UV-C stressed Chlamydomonas (ANOVA □ 0.05) including metabolites down-accumulated upon stress start related to central carbon and nitrogen metabolism (malic acid, citric acid, Ser, Glu) (a); early accumulated metabolites including phenolics (4-hydroxybenzoic acid), redox and carbon fixation-related (glycerol) and arabinose (b); and late accumulated sugars and flavonoids (catechin) (c).

Figure 4

sPLS-STRING sample plot. sPLS differentiated between harvesting times (a). sPLS based network overlapped to the STRING network including the protein nodes included in the sPLS based network. Resulting network showed the response differentiation between Chlamydomonas early and acclimation responses (b). Network nodes were colored according to their MapMan categories linking node size and the sPLS derived edge color to size and weight respectively. Only the sPLS derived edges with correlations higher or lower than ± 0.6 were visualized. Nodes without any edge above the threshold were removed from this analysis. Protein-protein STRING-derived edges were represented as dashed yellow lines.

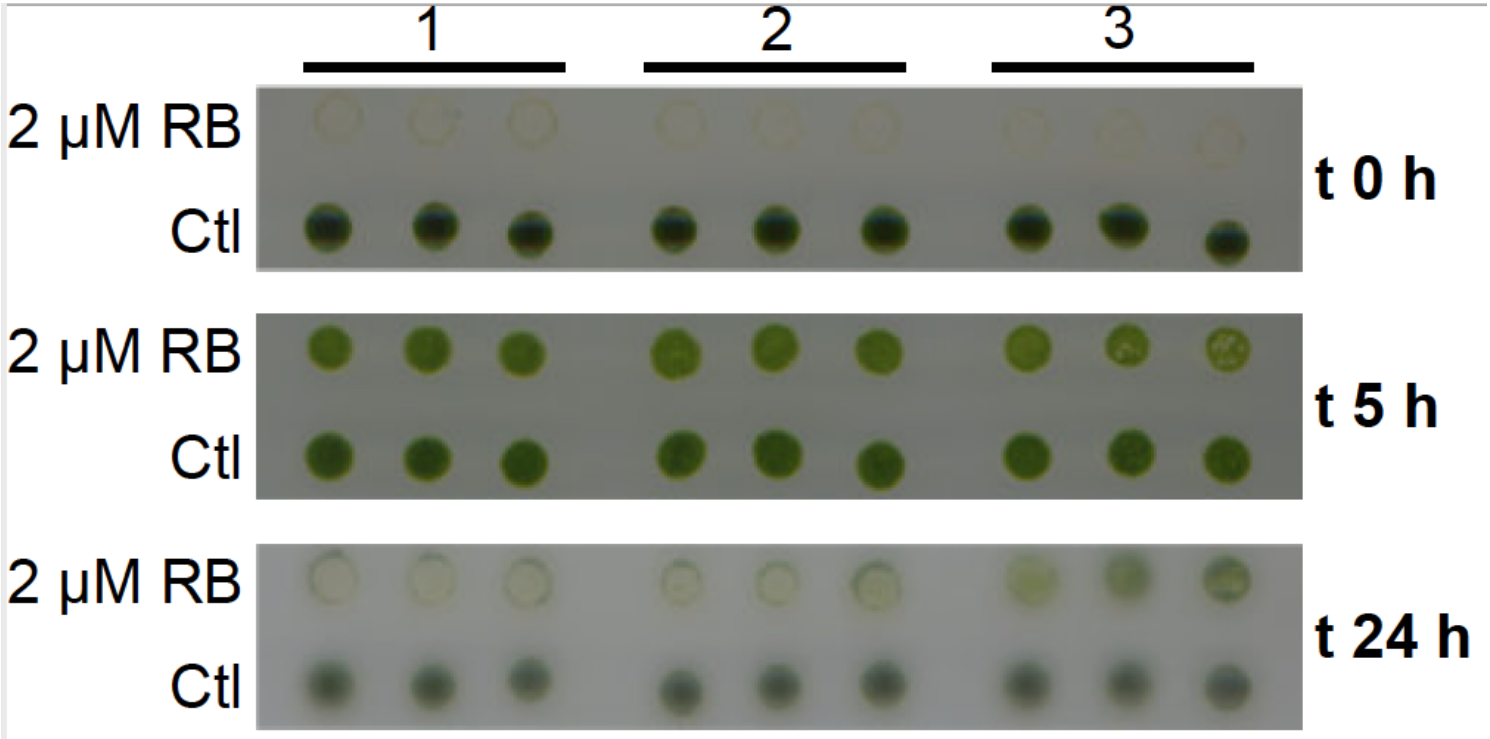

Figure 5

UV-C stress enhances Chlamydomonas tolerance to rose Bengal (RB)-induced singlet oxygen stress. Unstressed Chlamydomonas cultures were unable to grow after their exposition to 2 µM RB. Culture samples from the t 5 h harvest had an increased tolerance to RB induced oxidative stress with no differences in growth between untreated and 2 µM RB treated conditions. Tolerance to RB induced singlet oxygen stress was reduced in culture samples from the t 24 h as the RB treated samples grow less than the untreated ones.

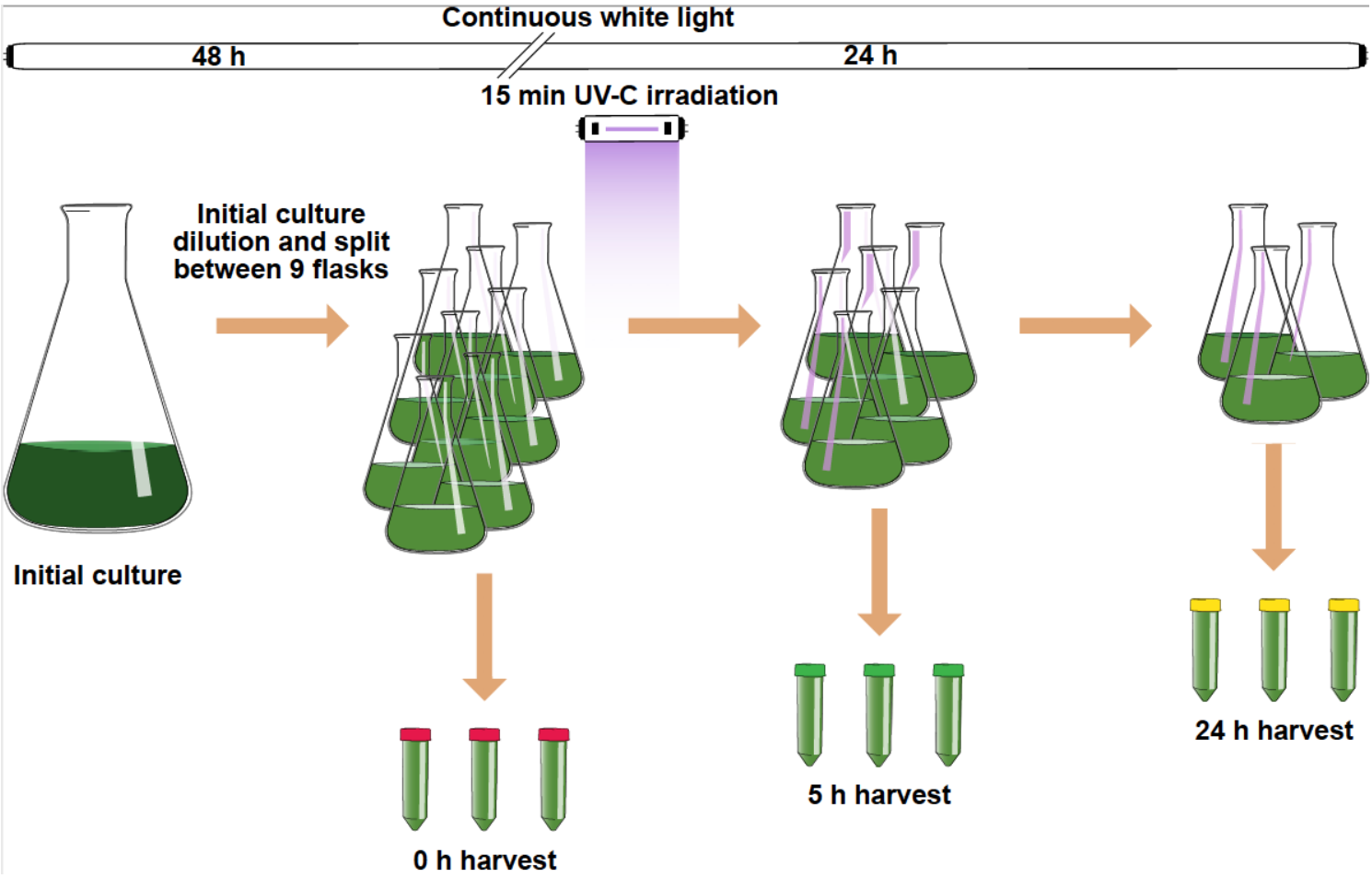

Figure 6

Experimental design. The initial Chlamydomonas culture grown under control conditions was diluted and split between nine flasks just before experiment start. Flasks were placed under continuous UV-C light irradiation during the first 15 min upon experiment start. Three different flasks were sampled for each harvesting time. Harvesting was performed at the experiment start (t 0 h), 5 and 24 h after UV-C irradiation start.

Supplementary Files

This is a list of supplementary files associated with this preprint. Click to download.

- Additionalfile2.pdf
- Additionalfile1.xlsx